

1 ***DrugEx v2: De Novo Design of Drug Molecule by Pareto-***
2 **based Multi-Objective Reinforcement Learning in**
3 **Polypharmacology**

4 Xuhan Liu¹, Kai Ye², Herman W. T. van Vlijmen^{1,3}, Michael T. M. Emmerich⁴, Adriaan
5 P. IJzerman¹, Gerard J. P. van Westen^{1, *}

6
7 ¹Drug Discovery and Safety, Leiden Academic Centre for Drug Research, Einsteinweg
8 55, Leiden, The Netherlands

9 ²School of electronics and information engineering, Xi'an Jiaotong University, 28
10 Xianning W Rd, Xi'an, China

11 ³Janssen Pharmaceutica NV, Turnhoutseweg 30, B-2340, Beerse, Belgium

12 ⁴Leiden Institute of Advanced Computer Science, Einsteinweg55, Leiden, The
13 Netherlands

14
15 *To whom correspondence should be addressed: Gerard J. P. van Westen, Drug
16 Discovery and Safety, Leiden Academic Centre for Drug Research, Einsteinweg 55,
17 Leiden, The Netherlands. Tel: +31-71-527-3511. Email: gerard@lacdr.leidenuniv.nl.

18
19 Email Address of other authors: (1) Xuhan Liu: x.liu@lacdr.leidenuniv.nl; (2) Kai Ye:
20 kaiye@xjtu.edu.cn; (3) Herman W. T. van Vlijmen: hvvlijme@its.jnj.com; (4) Michael
21 T. M. Emmerich: m.t.m.emmerich@liacs.leidenuniv.nl; (5) Adriaan P. IJzerman:
22 ijzerman@lacdr.leidenuniv.nl.

23

24 **Abbreviations**

ARs	Adenosine Receptors
DL	Deep Learning
MT-DNN	Multi-Task Deep Neural Network
ECFP	Extended Connectivity Fingerprint
EA	Evolutionary Algorithm
EDA	Estimation of Distribution Algorithm
GPCRs	G Protein-coupled Receptors
GRU	Gated Recurrent Unit
LSTM	Long Shot-Term Memory
QSAR	Quantitative Structure-Activity Relationship
RBF	Radial Basis Function
RMSE	Root Mean Square Error
ReLU	Rectified Linear Unit
RF	Random Forest
RL	Reinforcement Learning
RNNs	Recurrent Neural Networks
SVM	Support Vector Machine
t-SNE:	t-distributed Stochastic Neighbor Embedding

25

26

27 **Abstract**

28 In polypharmacology, ideal drugs are required to bind to multiple specific targets to
29 enhance efficacy or to reduce resistance formation. Although deep learning has
30 achieved breakthrough in drug discovery, most of its applications only focus on a single
31 drug target to generate drug-like active molecules in spite of the reality that drug
32 molecules often interact with more than one target which can have desired
33 (polypharmacology) or undesired (toxicity) effects. In a previous study we proposed a
34 new method named *DrugEx* that integrates an exploration strategy into RNN-based
35 reinforcement learning to improve the diversity of the generated molecules. Here, we
36 extended our *DrugEx* algorithm with multi-objective optimization to generate drug
37 molecules towards more than one specific target (two adenosine receptors, A₁AR and
38 A_{2A}AR, and the potassium ion channel hERG in this study). In our model, we applied
39 an RNN as the *agent* and machine learning predictors as the *environment*, both of which
40 were pre-trained in advance and then interplayed under the reinforcement learning
41 framework. The concept of evolutionary algorithms was merged into our method such
42 that *crossover* and *mutation* operations were implemented by the same deep learning
43 model as the *agent*. During the training loop, the agent generates a batch of SMILES-
44 based molecules. Subsequently scores for all objectives provided by the *environment*
45 are used for constructing Pareto ranks of the generated molecules with non-dominated
46 sorting and Tanimoto-based crowding distance algorithms. Here, we adopted GPU
47 acceleration to speed up the process of Pareto optimization. The final reward of each
48 molecule is calculated based on the Pareto ranking with the ranking selection algorithm.
49 The agent is trained under the guidance of the reward to make sure it can generate more
50 desired molecules after convergence of the training process. All in all we demonstrate
51 generation of compounds with a diverse predicted selectivity profile toward multiple
52 targets, offering the potential of high efficacy and lower toxicity.

53

54 **Keywords:** deep learning; adenosine receptors; cheminformatics; reinforcement
55 learning; multi-objective optimization; exploration strategy.

56

57 **Introduction**

58 The ‘one drug, one target, one disease’ paradigm, which has dominated the field of drug
59 discovery for many years, has made great contributions to drug development and the
60 understanding of their molecular mechanisms of action [1]. However, this strategy is
61 encountering problems due to the intrinsic promiscuity of drug molecules, *i.e.* recent
62 studies showed that one drug molecule could interact with six protein targets on average
63 [2]. Side effects of drugs caused by binding to unexpected off-targets are one of the
64 main reasons of clinical failure of drug candidates and even withdrawal of FDA-
65 approved novel drugs [3,4]. Up to now, more than 500 drugs have been withdrawn from
66 the market due to fatal toxicity [5]. Yet, disease often results from the perturbation of
67 biological systems by multiple genetic and/or environmental factors, thus complex
68 diseases are more likely to require treatment through modulating multiple targets
69 simultaneously. Therefore, it is crucial to shift the drug discovery paradigm to
70 “polypharmacology” for many complex diseases [6,7].

71

72 In polypharmacology, ideal drugs are required to bind to multiple specific targets to
73 enhance efficacy or to reduce resistance formation (in which case multiple targets can
74 be multiple mutants of a single target) [8]. It has been shown that partial inhibition of a
75 small number of targets can be more efficient than the complete inhibition of a single
76 target, especially for complex and multifactorial diseases [6,9]. In parallel, common
77 structural and functional similarity of proteins results in drugs binding to off-targets;
78 therefore we also demand drugs to have a high target selectivity to avoid binding to
79 unwanted target proteins. For example, the adenosine receptors (ARs) are a class of
80 rhodopsin-like G protein-coupled receptors (GPCRs) having adenosine as the
81 endogenous ligand. Adenosine and ARs are ubiquitously distributed throughout the
82 human tissues, and their interactions trigger a wide spectrum of physiological and
83 pathological functions. There are four subtypes of ARs, including A₁, A_{2A}, A_{2B} and A₃,
84 each of which has a unique pharmacological profile, tissue distribution, and effector
85 coupling [10,11]. The complexity of adenosine signaling and the widespread

86 distribution of ARs have always given rise to challenges in developing target-specific
87 drugs [12]. In addition to the similarity of the pharmacophores of some generic proteins
88 (*e.g.* human Ether-à-go-go-Related Gene, hERG) should also be taken into
89 consideration as they can be sensitive to binding exogenous ligands and cause side
90 effects. hERG is the alpha subunit of a potassium ion channel [13] and has an inclination
91 to interact with drug molecules because of its larger inner vestibule as the ligand binding
92 pocket [14]. When hERG is inhibited this may cause long QT syndrome [15].

93

94 In addition to visual recognition, natural language processing and gaming, deep
95 learning has been increasingly applied in drug discovery [16]. It does not only perform
96 well in prediction models for virtual screening, but is also used to construct generative
97 models for drug *de novo* design and/or drug optimization [17]. For example, our group
98 implemented a fully-connected deep neural network (DNN) to construct a
99 proteochemometric model (PCM) with all high quality ChEMBL data [18] for
100 prediction of ligand bioactivity [19]. Its performance was shown to be better than other
101 shallow machine learning methods. Moreover, we also developed a generative model
102 with recurrent neural networks (RNNs), named *DrugEx* for SMILES-based *de novo*
103 drug design [20]. It was shown that the generated molecules had large diversity and
104 were similar to known ligands to some extent to make sure that reliable and diverse
105 drug candidates can be designed.

106

107 Since the first version of *DrugEx* (*v1*) demonstrated effectiveness for designing novel
108 A_{2A}AR ligands, we began to extend this method for drug design toward multiple targets.
109 In this study, we updated *DrugEx* to the second version (*v2*) through merging crossover
110 and mutation operations, which were derived from evolutionary algorithms, into the
111 reinforcement learning (RL) framework. In order to evaluate the performance of our
112 additions we tested our method into both multi-target and target-specific cases. For the
113 multi-target case, desired molecules should have a high affinity towards both A₁AR and
114 A_{2A}AR. In the target-specific case, on the other hand, we required molecules to have
115 only high affinity towards the A_{2A}AR but a low affinity to the A₁AR for. In order to

116 decrease toxicity and adverse events, molecules were additionally obliged to have a low
117 affinity for hERG in both cases. It is worth noting that generated molecules should also
118 be chemically diverse and have similar physico-chemical properties to known ligands.
119 All python code for this study is freely available at
120 <http://github.com/XuhanLiu/DrugEx>.

121

122 **Materials and Methods**

123 **Data Source**

124 Drug like molecules represented as SMILES format were downloaded from the
125 ChEMBL database (version 26). After data preprocessing, including recombining
126 charges, removing metals and small fragments, we collected 1.7 million molecules and
127 named it the *ChEMBL* set, used for SMILES syntax learning. This data preprocessing
128 step was implemented in RDKit [21]. Furthermore, 25,731 ligands were extracted from
129 the ChEMBL database to construct the *LIGAND* set, which had bioactivity
130 measurements towards the human A₁AR, A_{2A}AR, and hERG. The *LIGAND* set was
131 used for constructing prediction models for each target and fine-tuning the generative
132 models. The number of ligands and bioactivities for these three targets in the *LIGAND*
133 set is represented in Table 1. Duplicate items were removed and if multiple
134 measurements for the same ligands existed, the average pChEMBL value (pX,
135 including pKi, pKd, pIC50, or pEC50) was calculated. To judge if a molecule is active
136 or not, we defined the threshold of bioactivity as pX = 6.5. If the pX < 6.5, the
137 compound was predicted as undesired (low affinity to the given target); otherwise, it
138 was regarded as desired (having high affinity) [19].

139

140 **Prediction Model**

141 In order to predict the pX for each generated molecule for a given target, regression
142 QSAR models were constructed with different machine learning algorithms. To
143 increase the chemical diversity available for the QSAR model we included lower
144 quality data without pChEMBL value, *i.e.* molecules that were labeled as “Not Active”

145 or without a defined pX value. For these data points we defined a pX value of 3.99
 146 (slightly smaller than 4.0) to eliminate the imbalance of the dataset and guarantee the
 147 model being able to predict the negative samples. During the training process, sample
 148 weights for low quality data were set as 0.1, while the data with exact pX were set as
 149 1.0. This allowed us to particularly incorporate the chemical diversity, while avoiding
 150 degradation of model quality. Descriptors used as input were ECFP6 fingerprints [22]
 151 with 2048 bits (2048 dimensions, or 2048D) calculated by the RDKit Morgan
 152 Fingerprint algorithm (using a three-bond radius). Moreover, the following 19D
 153 physico-chemical descriptors were used: molecular weight, logP, number of H bond
 154 acceptors and donors, number of rotatable bonds, number of amide bonds, number of
 155 bridge head atoms, number of hetero atoms, number of spiro atoms, number of heavy
 156 atoms, the fraction of SP3 hybridized carbon atoms, number of aliphatic rings, number
 157 of saturated rings, number of total rings, number of aromatic rings, number of
 158 heterocycles, number of valence electrons, polar surface area and Wildman-Crippen
 159 MR value. Hence, each molecule in the dataset was transformed into a 2067D vector.
 160 Before being input into the model, the value of input vectors were normalized to the
 161 range of [0, 1] by the MinMax method. Model output value is the probability whether
 162 a given chemical compound was active based on this vector.

163

164 **Table 1: The number of ligands and bioactivities for each of the human protein targets A₁AR,**
 165 **A_{2A}AR and hERG in the LIGAND set.**

	A ₁ AR	A _{2A} AR	hERG
Total Ligands	7700	8406	16733
Bioactivities	13100	12129	22156
Active Ligands (pX >= 6.5)	1990	2511	924
Inactive Ligands (pX < 6.5)	1859	1709	6438
Inactive Ligands (No pX)	1764	1993	1275
Other Ligands	2087	4704	8906

166

167 Four algorithms were benchmarked for QSAR model construction, Random Forest
168 (RF), Support Vector Machine (SVM), Partial Least Squares regression (PLS), and
169 Multi-task Deep Neural Network (MT-DNN). RF, SVM and PLS models were
170 implemented through Scikit-Learn [23], and the MT-DNN model through PyTorch [24].
171 In the RF, the number of trees was set as 1000 and split criterion was “gini”. In the
172 SVM, a radial basis function (RBF) kernel was used and the parameter space of C and
173 γ were set as $[2^{-5}, 2^{15}]$ and $[2^{-15}, 2^5]$, respectively. In the MT-DNN, the architecture
174 contained three hidden layers activated by a rectified linear unit (ReLU) between input
175 and output layers, and the number of neurons were 2048, 4000, 2000, 1000 and 3 in
176 these subsequent layers. The training process consisted of 100 epochs with 20% of
177 hidden neurons randomly dropped out between each layer. The mean squared error was
178 used to construct the loss function and was optimized by the Adam algorithm [25] with
179 a learning rate of 10^{-3} .

180

181 **Generative Model**

182 As in *DrugEx v1*, we organized the vocabulary for the SMILES construction. Each
183 SMILES-format molecule in the *ChEMBL* and *LIGAND* sets was split into a series of
184 tokens. Then all tokens existing in this dataset were collected to construct the SMILES
185 vocabulary. The final vocabulary contained 85 tokens (Table S1) which were selected
186 and arranged sequentially into valid SMILES sequences through correct grammar.

187

188 The RNN model constructed for sequence generation contained six layers: one input
189 layer, one embedding layer, three recurrent layers and one output layer. After being
190 represented by a sequence of tokens, molecules can be received as categorical features
191 by the input layer. In the embedding layer, vocabulary size, and embedding dimension
192 were set to 85 and 128, meaning each token could be transformed into a 128
193 dimensional vector. For a recurrent layer, the long-short term memory (LSTM) was
194 used as recurrent cell with 512 hidden neurons instead of the gated recurrent unit (GRU)
195 [26] which was employed only in *DrugEx v1*. The output at each position was the

196 probability that determined which token in the vocabulary would be chosen to grow the
197 SMILES string.

198

199 During the training process we put a start token (GO) at the beginning of a batch of data
200 as input and an end token (END) at the end of the same batch of data as output. This
201 ensures that our generative network could choose correct tokens each time based on the
202 sequence it had generated previously. A negative log likelihood function was used to
203 construct the loss function to guarantee that the token in the output sequence had the
204 largest probability to be chosen after being trained. In order to optimize the parameters
205 of the model, the Adam algorithm [25] was used for the optimization of the loss
206 function. Here, the learning rate was set at 10^{-3} , the batch size was 512, and training
207 steps were set to 1000 epochs.

208

209 **Reinforcement Learning**

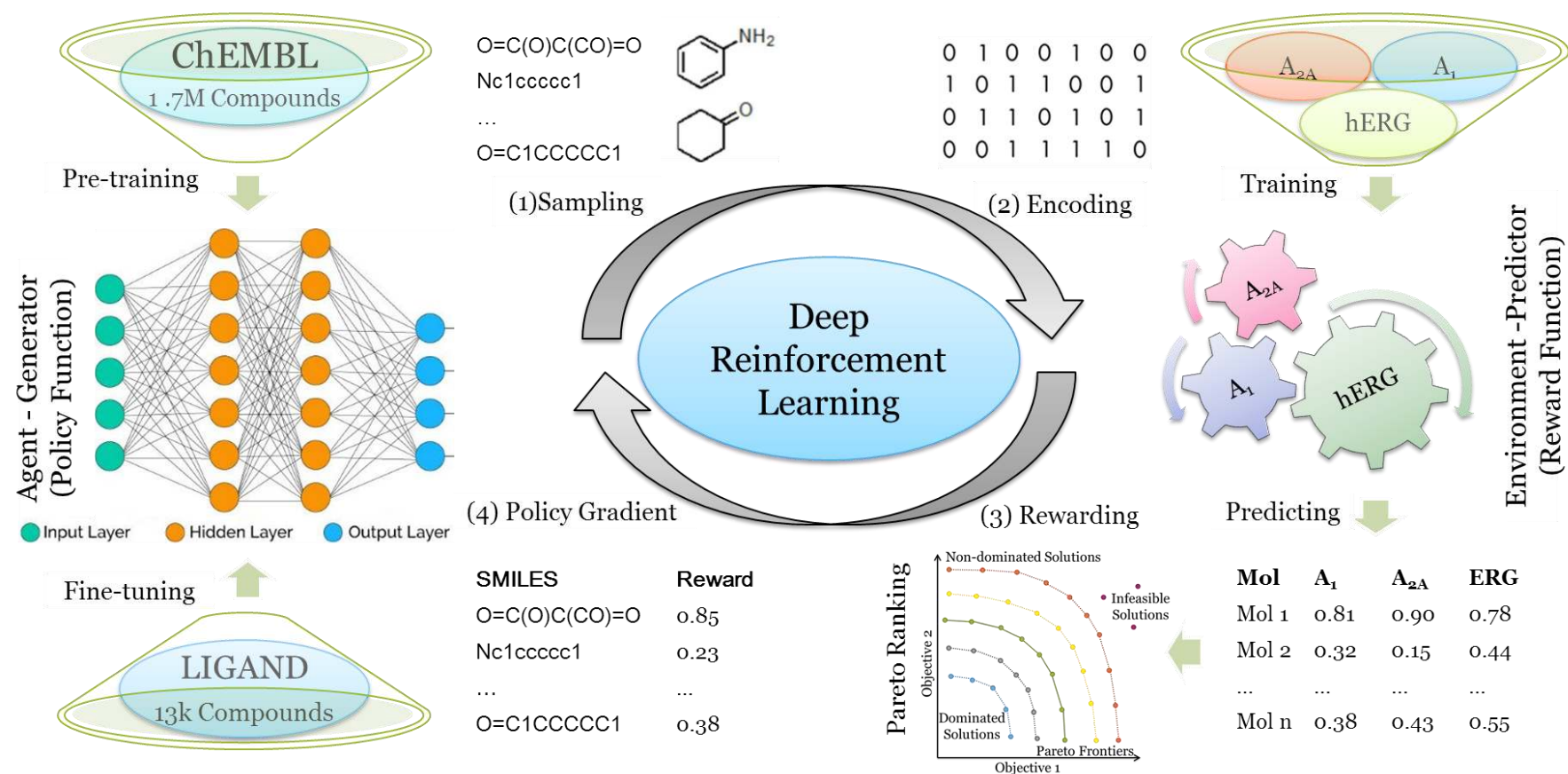
210 SMILES sequence construction under the RL framework can be viewed as a series of
211 decision-making steps (Fig. 1). The generator (G) and the predictors (Q) are regarded
212 as the policy and reward function, respectively. In this study we use multi-objective
213 optimization (MOO), and each objective is a requirement to be achieved maximally for
214 each scenario, albeit with differences in desirability. Our aim was defined by the
215 following problem statement:

$$216 \quad \text{maximize } R_1, \quad \text{maximize } R_2, \quad \dots, \quad \text{maximize } R_n$$

217 Here, n equals the number of objectives ($n = 3$ in this study), and R_i , the score for each
218 objective i , was calculated as follows:

$$219 \quad R_i = \begin{cases} \text{minmax}(pX_i), & \text{if high affinity required} \\ 1 - \text{minmax}(pX_i), & \text{if low affinity required} \\ 0, & \text{if SMILES invalid} \end{cases}$$

220



221

222 **Fig. 1: The workflow of the training process of our deep learning-based molecule generator *DrugEx2* utilizing reinforcement learning.** After the generator has
 223 been pre-trained/fine-tuned, (1) a batch of SMILES are generated by sampling tokens step by step based on the probability calculated by the generator;
 224 SMILES are parsed to be molecules and encoded into descriptors to get the predicted pXs with well-trained predictors; (3) The predicted pXs are transformed into a
 225 single value as the reward for each molecule based on Pareto optimization; (4) These SMILES sequences and their rewards are sent back to the generator for training
 226 with policy gradient methods. These four steps constitute the training loop of reinforcement learning.

227 here the pX_i (the range from 3.0 to 10.0) was the prediction score given by each
228 predictor for the i^{th} target, which was normalized to the interval [0, 1] as the reward
229 score. If having no or low affinity for a target was required (off-target) this score would
230 be subtracted from 1 (inverting it).

231

232 In order to evaluate the performance of the generators, three coefficients are calculated
233 with the generated molecules, including validity, desirability, and uniqueness which are
234 defined as:

$$\begin{aligned} \text{Validity} &= \frac{N_{valid}}{N_{total}} \\ \text{Desirability} &= \frac{N_{desired}}{N_{total}} \\ \text{Uniqueness} &= \frac{N_{unique}}{N_{total}} \end{aligned}$$

238 where N_{total} is the total number of molecules, N_{valid} is the number of the molecules parsed
239 by the valid SMILES sequences, N_{unique} is the number of molecules which are different
240 from others in the dataset, and $N_{desired}$ is the number of desired molecules. Here, we
241 determine if generated molecules are desired based on the reward R_i if all of them are
242 larger than the threshold (0.5 by default when $pX = 6.5$). In addition, we calculated SA
243 score (from 1 to 10) for each molecule to measure the synthesizability of which larger
244 value means more difficult to be synthesized. And we also computed QED (from 0 to
245 1) score to evaluate the drug-likeness of which larger value means more drug-like for
246 each molecule. The calculation of both SA and QED scores were implemented by
247 RDKit.

248

249 To orchestrate and combine these different objectives, we compared two different
250 reward schemes: the Pareto front (PF) scheme and the weighted sum (WS) scheme.

251 These were defined as follows:

252 **(a) Weighted sum (WS) scheme:** the weight for each function is not fixed but
253 dynamic, and depends on the desired ratio for each objective, which is defined as:

$$r_i = \frac{N_i^S}{N_i^I}$$

254

255 here for objective i the $N_i^<$ and $N_i^>$ are the number of generated molecules which have
256 a score smaller or larger than the threshold. Moreover, the weight is normalized ratio
257 defined as:

$$258 \quad w_i = \frac{r_i}{\sum_{k=1}^M r_k}$$

259 and the final reward R^* was calculated by

$$260 \quad R^* = \sum_{i=1}^n w_i R_i,$$

261 **(b) Pareto front (PF) scheme:** operates on the desirability score, which is defined as

$$262 \quad D_i = \begin{cases} 1, & \text{if } R_i > t_i \\ R_i/t_i, & \text{if } R_i \leq t_i \end{cases}$$

263 where t_i is the threshold of the i^{th} objective, and we set all of objectives had the same
264 threshold as 0.5 as stated in the methods. Given two solutions m_1 and m_2 with their
265 scores (x_1, x_2, \dots, x_n) and (y_1, y_2, \dots, y_n) , then m_1 is said to Pareto dominate m_2 if and only
266 if:

$$267 \quad \forall j \in \{1, \dots, n\}: x_j \geq y_j \text{ and } \exists j \in \{1, \dots, n\}: x_j > y_j$$

268 otherwise, m_1 and m_2 are non-dominated with each other. After the dominance between
269 all pair of solutions being determined, the non-dominated scoring algorithm [27] is
270 exploited to obtain a rank of Pareto frontiers which consist of a set of solutions. The
271 solutions in the top frontier are dominated by the other solutions in the bottom frontier,
272 but the solutions in the same frontier are non-dominated with each other [28]. In order
273 to speed up the non-dominated sorting algorithm, we employed *PyTorch* to implement
274 this procedure with GPU acceleration. After obtaining the frontiers ranking from
275 dominated solutions to dominant solutions, the molecules were ranked based on the
276 average of Tanimoto-distance instead of crowding distance with other molecules in the
277 same frontier, and molecules with smaller distances were ranked on the top. The final
278 reward R^* is defined as:

$$279 \quad R_i^* = \begin{cases} 0.5 + \frac{k - N_{undesired}}{2N_{desired}}, & \text{if desired} \\ \frac{k}{2N_{undesired}}, & \text{if undesired} \end{cases}$$

280 here the parameter k is the index of the solution in the Pareto rank, and rewards of

281 undesired and desired solutions will be evenly distributed in (0, 0.5] and (0.5, 0.1],
282 respectively.

283

284 During the generation process, for each step, G determines the probability of each token
285 from the vocabulary to be chosen based on the generated sequence in previous steps.
286 Its parameters are updated by employing a policy gradient based on the expected end
287 reward received from the predictor. The objective function is designated as follows:

$$288 \quad J(\theta) = \mathbb{E}[R^*(y_{1:T})|\theta] = \sum_{t=1}^T \log G(y_t|y_{1:t-1}) \cdot R^*(y_{1:T})$$

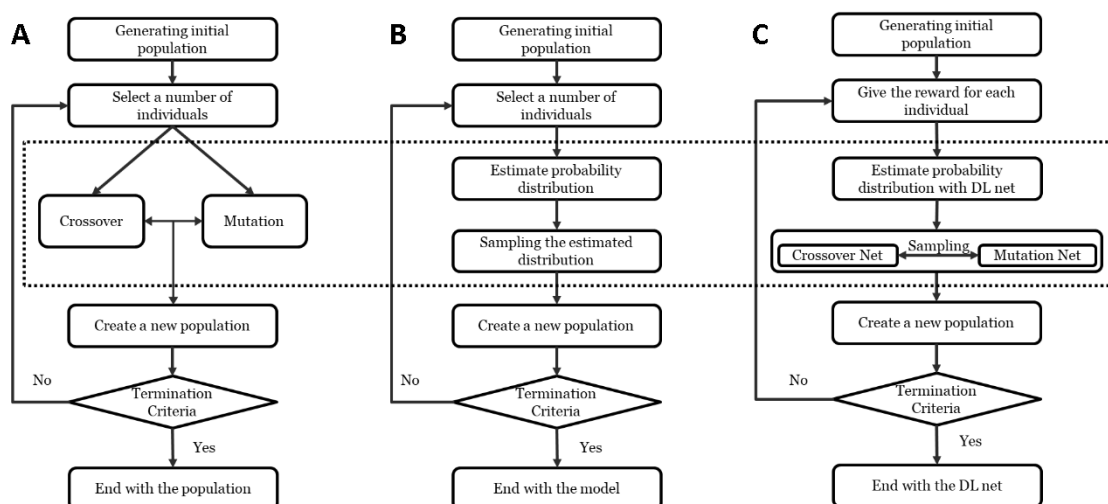
289 By maximizing this function, the parameters θ in G can be optimized to ensure that G
290 can construct desired SMILES sequences which can obtain the highest reward scores
291 judged by all the Q_s .

292

293 **Algorithm extrapolation**

294 Evolutionary algorithms (EAs) are common methods used in drug discovery [29]. For
295 example, *Molecule Evuator* is one of EAs, with mutation and crossover operations
296 based on SMILES representation [30] for drug *de novo* design. In addition, some groups
297 also proposed other variations of EAs [31], e.g., estimation of distribution algorithm
298 (EDA) which is a model-based method and replaces the *mutation* and *crossover*
299 operations with probability distribution estimation and sampling of new individuals
300 (Fig. 2) [32]. Similar to EDA, *DrugEx* is a model-based method too, in which the deep
301 learning model was employed to estimate the probability distribution of sequential
302 decision making. However, we use a DL method to define model-based *mutation* and
303 *crossover* operations. Moreover, we employed an RL method to replace the sample
304 selection step for the update of model or population in EDA or EA, respectively.

305



306

307 **Fig. 2: Flowchart comparison of evolutionary algorithm (A), estimation of distribution**
 308 **algorithm (B) and our proposed method (C).**

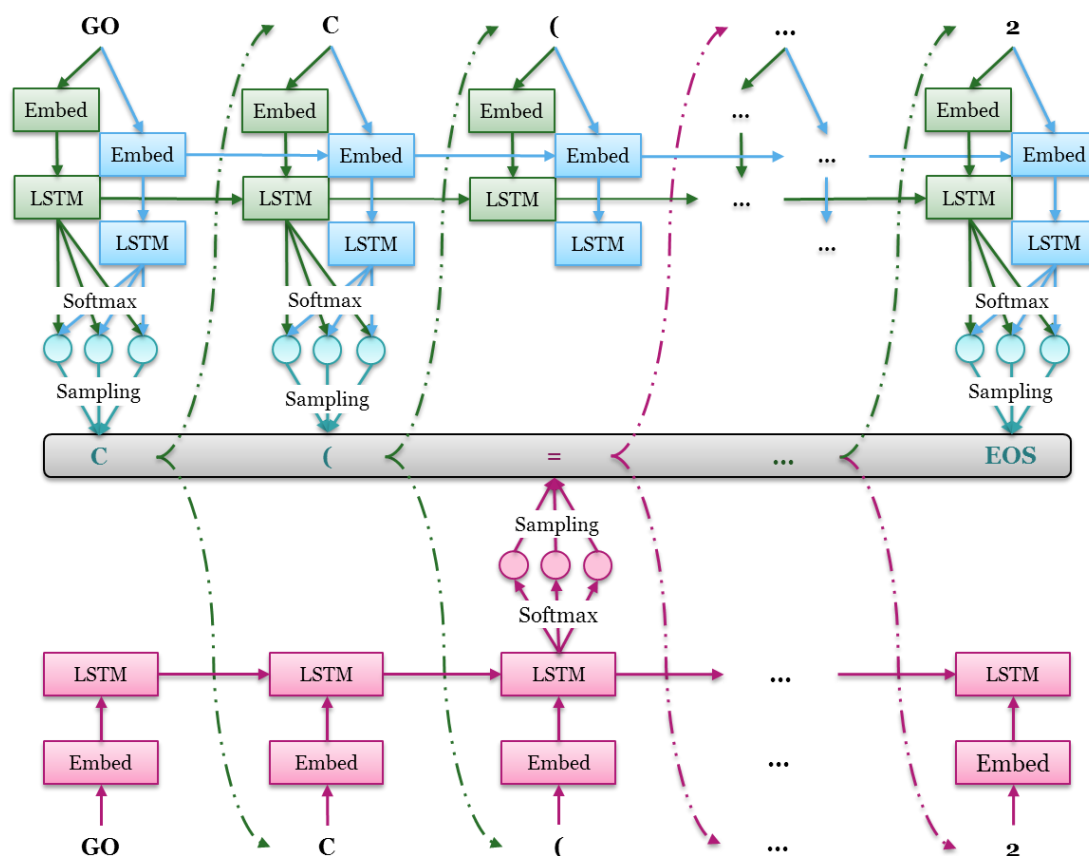
309

310 Exploration Strategy

311 In our previous study, we had implemented the exploration strategy through importing
 312 a fixed exploration net to enlarge the diversity of the generated molecules during the
 313 training loops. In this study, we continued to extend the methods of this exploration
 314 strategy, which resemble the *crossover* and *mutation* operations from evolutionary
 315 algorithms (EAs). Here, besides the *agent* net (G_A), we also defined exploration strategy
 316 with two other DL models: *crossover* net (G_C) and *mutation* net (G_M), which have the
 317 same RNN architecture (Fig. 3). Before the training process, they were initialized by a
 318 pre-trained or fine-tuned model. The G_M was the basic strategy employed in the
 319 previous version and its parameters were fixed and not updated during the whole
 320 training process. The G_C implemented in this work was an extended strategy whose
 321 parameters were updated iteratively based on the G_A . During the training process, each
 322 SMILES sequence was generated through combining these three RNNs: for each step,
 323 a random number from 0 to 1 is generated. If it is larger than the mutation rate (ϵ), the
 324 probability for token sampling is controlled by the combination of G_A and G_C , otherwise,
 325 it is determined by G_M . For each training loop, only the parameters in G_A were updated
 326 instantly based on the gradient of the RL objective function. An iteration was defined
 327 as the period of epochs after the desirability score of molecules generated by G_A did not
 328 increase. Subsequently the parameters of G_C were updated with G_A directly and the

329 training process continued for the next iteration. The training process would continue
 330 till the percentage of desired molecules in the current iteration was not better than in
 331 the previous iterations.

332



333

334 **Fig. 3: The mechanism of updated exploration strategy, including agent net G_A , mutation net**
 335 **G_M (red) and crossover net G_C (blue).** In the training loop, G_M is fixed, G_C is updated iteratively
 336 and G_A is trained at each epoch. For each position, a random number from 0 to 1 is generated. If it
 337 is larger than the mutation rate (ϵ), the probability for token sampling is controlled by the
 338 combination of G_A and G_C , otherwise, it is determined by G_M .

339

340 **Molecular Diversity**

341 To measure molecular diversity, we adopted the metric proposed by Solow and Polasky
 342 in 1994 to estimate the diversity of a biological population in an eco-system [33]. It has
 343 been shown to be an effective method to measure the diversity of drug molecules [34].
 344 The formula to calculate diversity was redefined to normalize the range of values from
 345 [1, m] to (0, m] as follows:

346

$$I(A) = \frac{1}{|A|} e^{\top F(s)^{-1} e}$$

347 where A is a set of drug molecules with a size of $|A|$ equal to m , \mathbf{e} is an m -vector of 1's
348 and $F(\mathbf{s}) = [f(d_{ij})]$ is a non-singular $m \times m$ distance matrix, in which $f(d_{ij})$ stands for
349 the distance function of each pair of molecule provided as follows:

$$352 \quad f(d) = e^{-\theta d_{ij}}$$

350 here we defined the distance d_{ij} of molecules s_i and s_j by using the Tanimoto-distance
351 with ECFP6 fingerprints as follows:

$$353 \quad d_{ij} = d(s_i, s_j) = 1 - \frac{|s_i \cap s_j|}{|s_i \cup s_j|},$$

354 where $|s_i \cap s_j|$ represents the number of common fingerprint bits, and $|s_i \cup s_j|$ is the
355 number of union fingerprint bits.

356

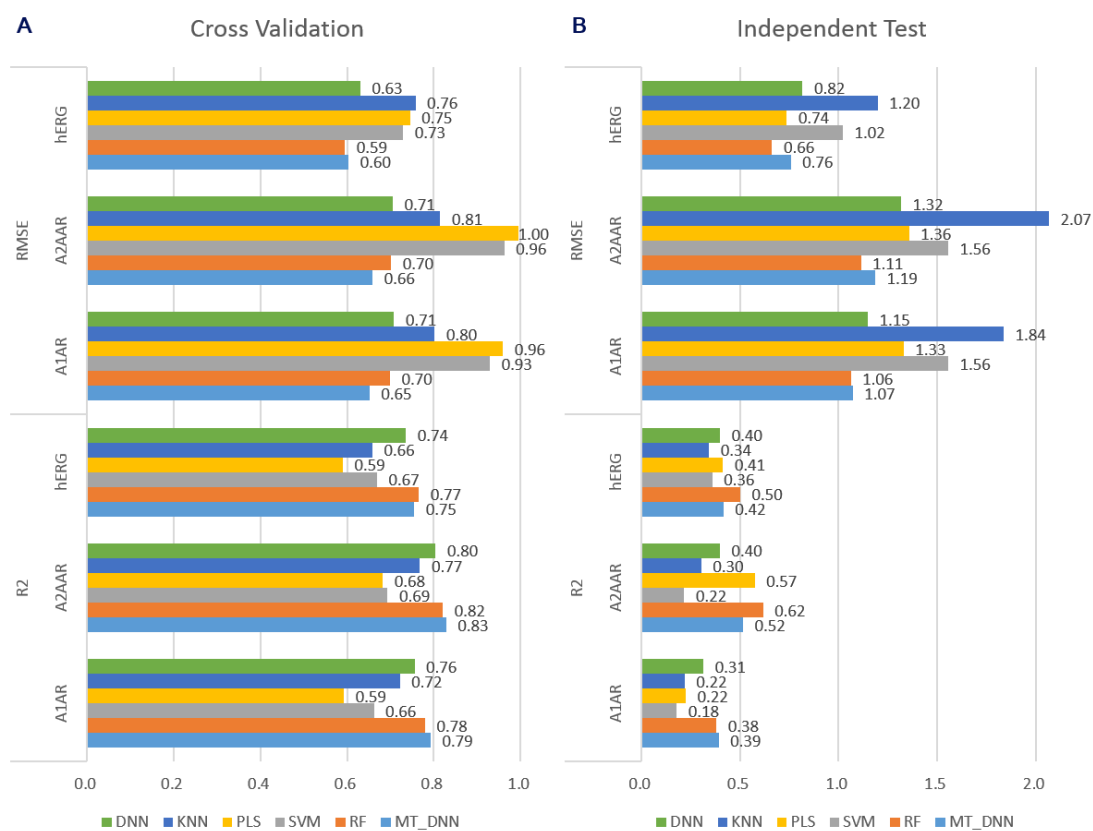
357 **Results and Discussion**

358 **Performance of Predictors**

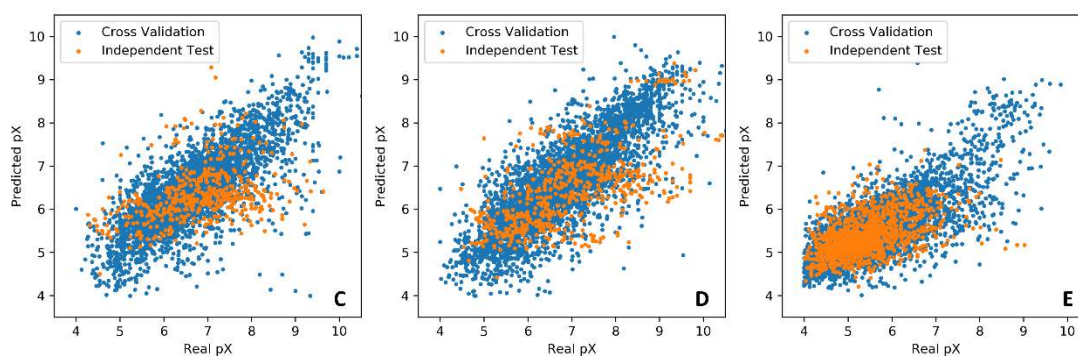
359 All molecules in the *LIGAND* set were used to train the QSAR models, after being
360 transformed into predefined descriptors, including 2048D ECFP6 fingerprints and 19D
361 physicochemical properties. We then tested the performance of these different
362 algorithms with five-fold cross validation and an independent test of which the
363 performances are shown in Fig. 4AB. Here, the dataset was randomly split into five
364 folds in the cross validation, while a temporal split with a cut-off at the year of 2015
365 was used for the independent test. In the cross validation test, the MT-DNN model
366 achieved the highest value for R^2 and the lowest RMSE value for A_{1AR} and A_{2AAR} ,
367 but the RF model had the best performance for hERG based on R^2 and RMSE. However,
368 for the independent test the RF model reached the highest R^2 and lowest RMSE across
369 the board, although it was worse than the performance in the cross-validation test. A
370 detailed performance overview of the RF model is shown in Fig. 4C-E. Because the
371 generative model might create a large number of novel molecules, which would not be
372 similar to the molecules in the training set, we took the robustness of the predictor into
373 consideration. In this situation the temporal split has been shown to be more robust
374 [19,35]. Hence the RF algorithm was chosen for constructing our environment which

375 provides the final reward to guide the training of the generator in RL.

376



377



378

379 **Fig. 4: Performance comparison of different machine learning regression models.** In these two

380 histograms (A-B), the results were obtained based on five-fold cross validation (A) and independent

381 test (B) for the three targets. The R^2 and RMSE scores were used to evaluate the performance of

382 different machine learning models including DNN, KNN, PLS, SVM RF and MT-DNN. In the

383 scatter plots (C-E), each point stands for one molecule with its real pX (x -axis) and the predicted

384 pX (y -axis) by the RF model which was chosen as the final predictors for A₁AR (C), A₂AAR (D)

385 and hERG (E) based on five-fold cross validation (blue) and independent test (orange).

386

387 **Model optimization**

388 As in our previous work in *DrugEx v1*, we firstly pre-trained and fine-tuned the
389 generator with the *ChEMBL* and *LIGAND* set, respectively. When testing the different
390 types of RNNs, we analyzed the performance of the pre-trained model with 10,000
391 SMILES generated, and found that LSTM generated more valid SMILES (97.5%) than
392 GRU (93.1%) which had been adopted in our previous work. Moreover, for the fine-
393 tuning process, we split the *LIGAND* set into two subsets: training set and validation
394 set; the validation set was not involved in parameters updating but it was essential to
395 avoid model overfitting and to improve uniqueness of generated molecules.
396 Subsequently 10,000 SMILES were sampled for performance evaluation. We found
397 that the percentage valid SMILES was 97.9% for LSTM, larger than GRU with 95.7%
398 valid SMILES, a slight improvement compared to the pre-trained model. In the end, we
399 employed the LSTM-based pre-trained/fine-tuned models for the following
400 investigation.

401

402 We employed the models for two cases (multi-target and target-specific) of multi-
403 objective drug design towards three protein targets. During the training loop of *DrugEx*
404 *v2*, the parameter of ϵ was set to different values: 10^{-2} , 10^{-3} , 10^{-4} and we also tested it
405 without mutation net, *i.e.* the value of ϵ was set to 0. Generators were trained by using
406 a policy gradient with two different rewarding schemes. After the training process
407 converged, 10,000 SMILES were generated for each model for performance evaluation.
408 The percentage of valid, desired, unique desired SMILES and the diversity were
409 calculated (Table 2). Furthermore, we also compared the chemical space of these
410 generated molecules with known ligands in the *LIGAND* set. Here, we employed first
411 two components of t-SNE on the ECFP6 descriptors of these molecules to represent the
412 chemical space.

413

414 **Performance comparisons**

415 We compared the performance of *DrugEx v2* with *DrugEx v1* and two other DL-based
416 *de novo* drug design methods: *REINVENT* [36] and *ORGANIC* [37]. In order to make

417 a fair benchmark, we trained these four methods with the same environments to provide
418 the unified predicted bioactivity scores for each of the generated molecules. It should
419 be mentioned that these methods are all SMILES-based RNNs generators but trained
420 under different RL frameworks. Therefore, these generators were constructed with the
421 same RNN structures of and initialized with the same pre-trained/fine-tuned models.

422

423 In the WS scheme we did not choose fixed weights for objectives but dynamic values
424 which can be adjusted automatically during the training process. The reason for this is
425 that if the fixed weights should be optimized as the hyperparameters, which would be
426 more time consuming. Moreover, the distribution of scores for each objective was not
427 comparable. If the affinity score was required to be higher, few of the molecules
428 generated by the model with initial state were satisfactory, but if a lower affinity score
429 was required, most of the generated molecules by the pre-trained/fine-tuned model met
430 this need without further training of RL. Therefore, weights were set as dynamic
431 parameters and determined by the ratio between desired and undesired molecules
432 generated by the model at the current training step. This approach ensures that the
433 objectives with lower scores would get more importance than others during the training
434 loop to balance the different objectives and generate more desired molecules.

435

436 The performance of the model with different ϵ is shown in Table S2. A higher ϵ
437 generates molecules with larger diversity but low desirability compared to a lower ϵ in
438 both multi-target and target-specific cases. In addition, an appropriate ϵ guarantees the
439 model generates molecules which have a more similar distribution of important
440 substructures with the desired ligands in the *LIGAND* set. With the WS scheme, the
441 model generates molecules with a high desirability, but the diversity is lower than the
442 desired ligands in the training set. On the contrary, the PF scheme helped the model
443 generate molecules with a larger diversity than the ligands in the training set, but the
444 desirability was not as high as in the WS rewarding scheme. Moreover, the generated
445 molecules in the PF scheme have more similar distribution of substructures to the
446 *LIGAND* set than in the WS scheme.

447

448 **Table 2: Comparison of validity, desirability, uniqueness and substructure distributions of**
 449 **SMILES generated by four different methods in the multi-target case with PF and WS**
 450 **rewarding schemes, respectively.** For the validity, desirability and uniqueness, the largest data is
 451 bold, while for the distribution of substructures, the bold data are labeled as the most closed to the
 452 values in the *LIGAND* set.

Rewarding Scheme	Dataset	Validity	Desirability	Uniqueness	Diversity	Purine Ring	Furan Ring	Benzene Ring
	<i>LIGAND</i>	100.00%	12.40%	100.00%	0.66	21.30%	35.44%	79.24%
PF	<i>DrugEx v1</i>	98.28%	43.27%	88.96%	0.71	17.37%	41.05%	80.95%
	<i>DrugEx v2</i>	99.57%	80.81%	87.29%	0.7	13.97%	32.01%	80.26%
	<i>ORGANIC</i>	98.84%	66.01%	82.67%	0.65	17.27%	56.38%	68.87%
	<i>REINVENT</i>	99.54%	57.43%	98.84%	0.77	0.64%	40.38%	92.05%
WS	<i>DrugEx v1</i>	97.76%	38.44%	93.44%	0.71	10.76%	36.42%	86.99%
	<i>DrugEx v2</i>	99.80%	97.45%	89.08%	0.49	3.63%	21.06%	96.18%
	<i>ORGANIC</i>	99.08%	61.10%	77.65%	0.68	9.08%	70.99%	83.91%
	<i>REINVENT</i>	99.54%	70.98%	99.11%	0.71	0.04%	23.23%	96.28%

453

454 In the multi-target case, these four methods with different rewarding schemes show
 455 similar performance, *i.e.* the WS scheme can help models improve the desirability while
 456 the PF scheme assists models to achieve better diversity and distribution of
 457 substructures (Table 2). Here, *REINVENT* with the PF scheme achieved the largest
 458 diversity, whereas *DrugEx v1* had the most similar substructure distribution to the
 459 molecules in the *LIGAND* set, and *DrugEx v2* achieved the best desirability with both
 460 PR and WS schemes compared to the three other algorithms. The diversity and
 461 distribution of substructures were also most similar to the best results. In addition, in
 462 the target-specific case results were similar to the multi-target case, (Table 3), and for
 463 the distribution of purine and furan rings, *DrugEx v2* surpassed *v1* to be most similar
 464 to the *LIGAND* set. When investigating the SA and QED scores, we observed that PF
 465 scheme helped all of generated molecules being more drug-like because of higher QED
 466 scores than WS scheme in both multi-target case (Fig. 6A-D) and target-specific case
 467 (Fig. 6E-H). In comparison of these methods, the molecules generated by *REINVENT*
 468 were supposedly easier to be synthesized and more drug-like than others, but the

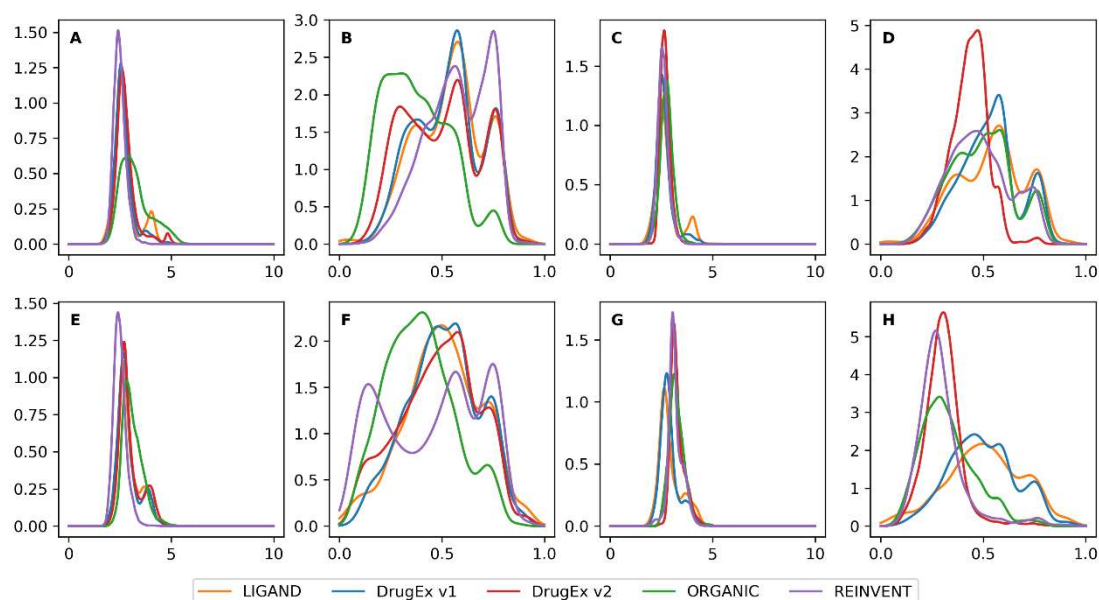
469 molecules of *DrugEx v1* had more similar distributions with the molecules in the
 470 *LIGAND* set.

471

472 **Table 3: Comparison of validity, desirability, uniqueness and substructure distributions of**
 473 **SMILES generated by four different methods in the target-specific case with PF and WS**
 474 **rewarding schemes, respectively.** For the validity, desirability and uniqueness, the largest data is
 475 bold, while for the distribution of substructures, the bold data are labeled as the most closed to the
 476 values in the *LIGAND* set.

Rewarding Scheme	Dataset	Validity	Desirability	Uniqueness	Diversity	Purine Ring	Furan Ring	Benzene Ring
	<i>LIGAND</i>	100.00%	14.63%	100.00%	0.67	28.27%	50.61%	71.84%
PF	<i>DrugEx v1</i>	98.07%	48.42%	87.32%	0.73	29.65%	61.61%	70.99%
	<i>DrugEx v2</i>	99.53%	89.49%	90.55%	0.73	23.73%	56.23%	67.40%
	<i>ORGANIC</i>	98.29%	86.98%	80.30%	0.64	10.60%	89.27%	65.28%
	<i>REINVENT</i>	99.59%	70.66%	99.33%	0.79	3.85%	33.82%	92.53%
WS	<i>DrugEx v1</i>	97.61%	44.96%	95.89%	0.68	78.92%	80.21%	68.02%
	<i>DrugEx v2</i>	99.62%	97.86%	90.54%	0.31	19.58%	98.56%	51.87%
	<i>ORGANIC</i>	98.97%	88.14%	84.13%	0.49	9.68%	96.66%	71.48%
	<i>REINVENT</i>	99.55%	81.27%	98.87%	0.34	25.13%	97.52%	74.61%

477



478

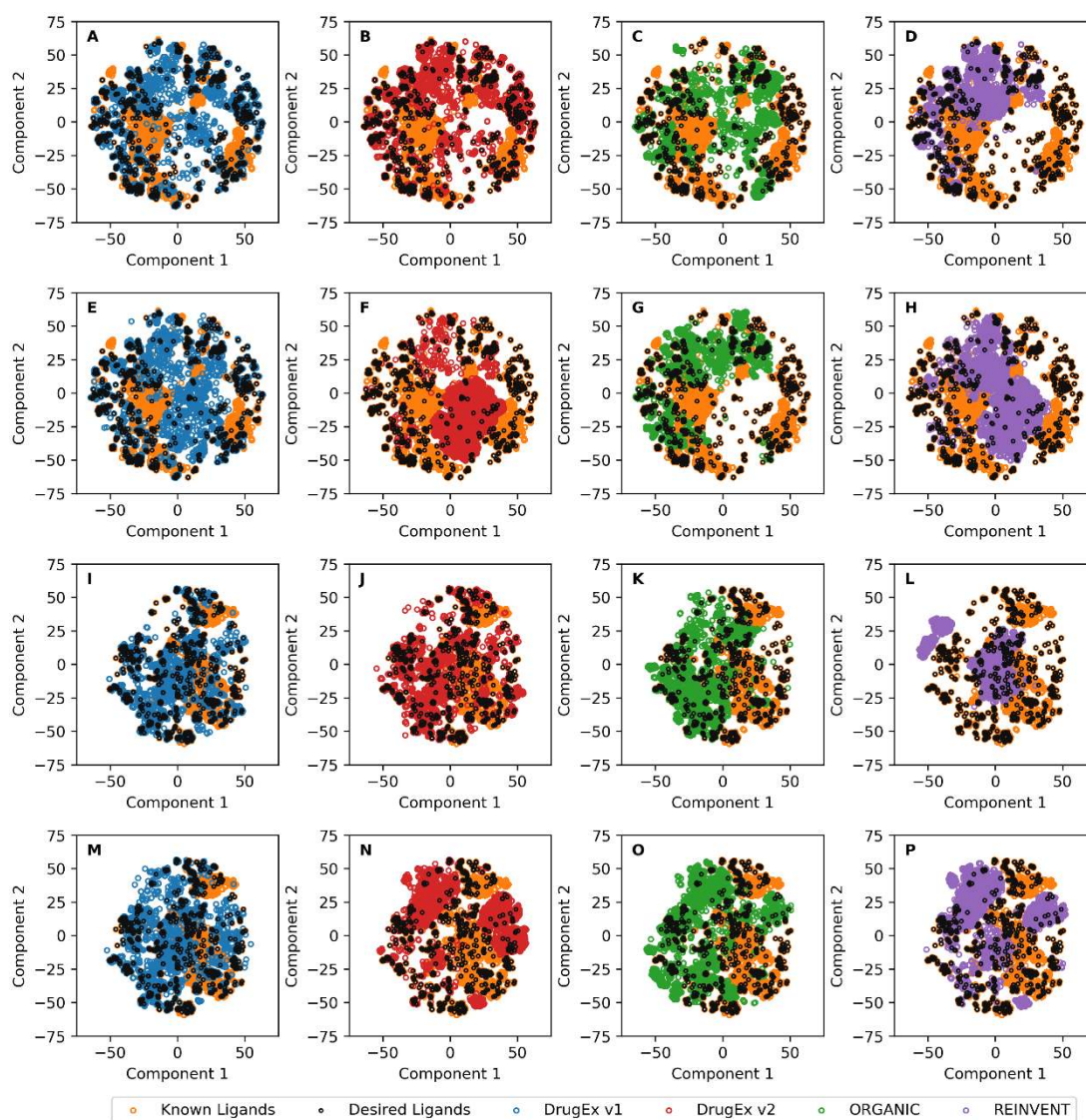
479 **Fig. 5: the distribution of SA score and QED score of desired ligands in the *LIGAND* set and**
 480 **of molecules generated by four different methods with PR (A, B, E and F) and WS (C, D, G**
 481 **and H) rewarding schemes in the multi-target case (A-D) and target-specific case (E-H). The**

482 molecules from the *LIGAND* set were shown as color of orange, and the molecules generated by
483 *DrugEx v1*, *v2*, *ORGANIC* and *REINVENT* were represented with colors of blue, green, red, and
484 purple, respectively. Overall *DrugEx v1* and *v2* are better able to emulate the observed distributions
485 in the training set compared to *ORGANIC* and *REINVENT*.

486

487 With respect to chemical space, we employed t-SNE with the ECFP6 descriptors of all
488 molecules for both multi-target (Fig. 6A-H) and target-specific cases (Fig. 6I-P). In the
489 multi-target case, most of desired ligands in the *LIGAND* set were distributed in the
490 margin and PR scheme could guide all of the generators to search more regions than
491 WS scheme. In the target-specific case, the desired ligands in the *LIGAND* set were
492 distributed more dispersed in both of the margin and the center regions. However, PF
493 scheme was not shown the similar results as in the target-specific case to improve the
494 coverage compared with WS scheme except for *DrugEx v2*. For both of these two cases,
495 only part of the region occupied by desired ligands in the *LIGAND* set were overlapped
496 with *REINVENT* and *ORGANIC*, but almost all of it is covered by *DrugEx v1* and *v2*.
497 Especially, in contrast to WS scheme *DrugEx v2* had a significant improvement of
498 chemical space coverage with PF scheme. A possible reason is that the molecules
499 generated by *DrugEx v1* and *v2* offer a more similar distribution of substructures to
500 desired ligands in the *LIGAND* set than *REINVENT* and *ORGANIC*.

501



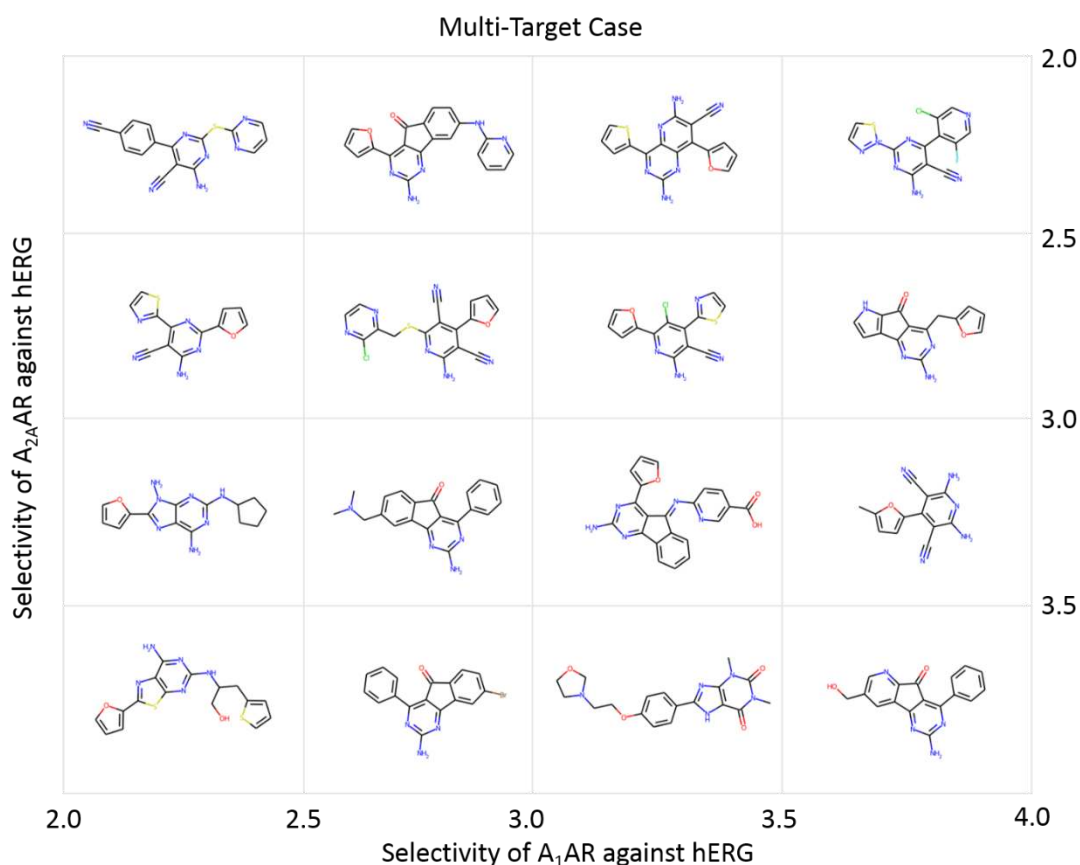
502

503 **Fig. 6: Comparison of the chemical space of ligands in the *LIGAND* set (orange for all**
 504 **molecules and black for desired molecules) and of generated molecules by *DrugEx v1* (A, E, I,**
 505 **M, blue), *v2* (B, F, J, N, red), *ORGANIC* (C, G, K, O, green) and *REINVENT* (D, H, L, P,**
 506 **purple), for the multi-target case (A-H) and target specific case (I-P). Chemical space is**
 507 **represented by the first two components in t-SNE with ECFP6 descriptors of molecules. The first**
 508 **and third rows were obtained with PF rewarding scheme, and the second and fourth rows were**
 509 **obtained with WS rewarding scheme. Similar to our previous work it can be seen that DrugEx better**
 510 **covers the whole chemical space of the input data. In particular in the multi-target case with a pareto**
 511 **optimization based scoring function (E-H) the improved coverage in all sections, including isolated**
 512 **active ligands, becomes clear.**

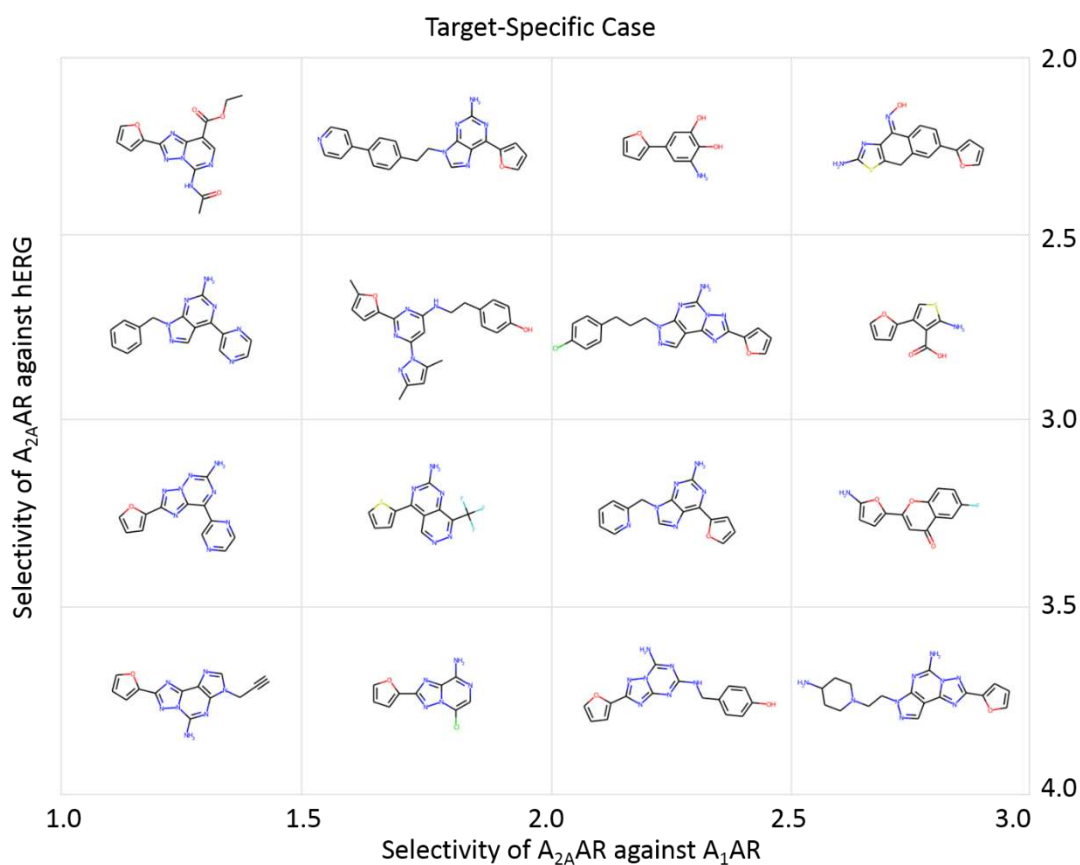
513

514

515 As an example, 16 possible antagonists (without ribose moiety and molecular weight <
516 500) generated by *DrugEx v2* with PR scheme were selected as candidates for both
517 multi-target cases and target specific case, respectively. These molecules were ordered
518 by the selectivity which was calculated as the difference of pXs between two different
519 protein targets. In the multi-target cases (Fig. 7A), because the desired ligands prefer
520 A₁AR and A_{2A}AR to hERG, the row and column is the selectivity of A_{2A}AR and A₁AR
521 against hERG, respectively, while the generated molecules are required to bind only
522 A_{2A}AR rather than A₁AR and hERG in the target-specific case (Fig. 7B), selectivity of
523 A_{2A}AR against A₁AR and hERG were represented as the row and column, respectively.
524



525



526

527 **Fig. 7: Some candidate molecules were selected from molecules generated by *DrugEx v2* with**
 528 **PR scheme for both multi-target case and target-specific case. In multi-target case (A), these**
 529 **molecules were ordered by the selectivity of A_1AR and $A_{2A}AR$ against hERG as x -axis**
 530 **and y -axis, respectively. In target-specific case (B), these molecules were ordered by**
 531 **the selectivity of $A_{2A}AR$ against A_1AR and hERG as x and y -axis, respectively.**

532

533 In order to prove the effectiveness of our proposed method, we tested it with 20 goal-
 534 directed molecule generation tasks on the GuacaMol benchmark platform [38]. These
 535 tasks contain different requirements, including similarity, physicochemical properties,
 536 isomerism, scaffold matching, *etc.* The detailed description of these tasks is provided
 537 in ref [38] and our results are shown in Table S3. We pre-trained our model with the
 538 dataset provided by the GuacaMol platform, in which all molecules from the ChEMBL
 539 database are included and similar molecules to the target ligands in the tasks were
 540 removed. Then we choose the top 1024 molecules in the training set to fine-tune our
 541 model for each task, before reinforcement learning was started. Our method scores the

542 best in 12 out of 20 tasks compared with the baseline models provided by the GuacaMol
543 platform, leading to an overall second place. Moreover, the performance between the
544 LSTM benchmark method and our methods were similar in these tasks, possibly
545 because they have similar architectures of neural networks. All in all, this benchmark
546 demonstrated that our proposed method has improved generality for drug *de novo*
547 design tasks. It is worth being mentioned that our method is not effective enough yet
548 for some tasks of contradictory objectives in the narrow chemical space. The main
549 reason is that our method emphasizes to obtain a large number of feasible molecules to
550 occupy the diverse chemical space rather than small number of optimal molecules to
551 achieve the highest score. For example, in the *Sitagliptin MPO task*, the aim is finding
552 molecules which are dissimilar to sitagliptin but have a similar molecular formula to
553 sitagliptin, and our method was not as good as Graph GA, which is a graph-based
554 genetic algorithm.

555

556 **Conclusion and Future Prospects**

557 In this work, we proposed a Pareto-based multi-objective learning algorithm for drug
558 *de novo* design towards multiple targets based on different requirements of affinity
559 scores for multiple targets. We transferred the concept of an evolutionary algorithm
560 (including mutation and crossover operations) into RL to update *DrugEx* for multi-
561 objective optimization. In addition, Pareto ranking algorithms were also integrated into
562 our model to handle the contradictory objectives common in drug discovery and enlarge
563 the chemical diversity. In order to prove effectiveness, we tested the performance of
564 *DrugEx v2* in both multi-target and target-specific cases. We found that a large
565 percentage of generated SMILES were valid and desired molecules without many
566 duplications. Moreover, the generated molecules were also similar to known ligands
567 and covered almost every corner of the chemical space that known ligands occupy,
568 which could not be repeated by tested competing methods. In future work, we will try
569 the generality of our proposed methods with different molecular representations, such
570 as graphs or fragments [29]. We will also integrate more objectives (e.g. stability,

571 synthesizability), especially when these objectives are contradictory, such that the
572 model allows user-defined weights for each objective to generate more reliable
573 candidate ligands and better steer the generative process.

574 **Authors' Contributions**

575 XL and GJPvW conceived the study and performed the experimental work and analysis.
576 KY, APIJ, ME and HWTvV provided feedback and critical input. All authors read,
577 commented on and approved the final manuscript.

578

579 **Acknowledgements**

580 XL thanks Chinese Scholarship Council (CSC) for funding, GJPvW thanks the Dutch
581 Research Council and Stichting Technologie Wetenschappen (STW) for financial
582 support (STW-Veni #14410).

583

584 **Competing Interests**

585 The authors declare that they have no competing interests

586

587

588 **Reference**

- 589 1. Chaudhari R, Tan Z, Huang B, Zhang S (2017) Computational polypharmacology: a new
590 paradigm for drug discovery. *Expert Opin Drug Discov* 12 (3):279-291.
591 doi:10.1080/17460441.2017.1280024
- 592 2. Giacomini KM, Krauss RM, Roden DM, Eichelbaum M, Hayden MR, Nakamura Y (2007)
593 When good drugs go bad. *Nature* 446 (7139):975-977. doi:10.1038/446975a
- 594 3. Lounkine E, Keiser MJ, Whitebread S, Mikhailov D, Hamon J, Jenkins JL, Lavan P, Weber E,
595 Doak AK, Cote S, Shoichet BK, Urban L (2012) Large-scale prediction and testing of drug
596 activity on side-effect targets. *Nature* 486 (7403):361-367. doi:10.1038/nature11159
- 597 4. Cook D, Brown D, Alexander R, March R, Morgan P, Satterthwaite G, Pangalos MN (2014)
598 Lessons learned from the fate of AstraZeneca's drug pipeline: a five-dimensional framework.
599 *Nat Rev Drug Discov* 13 (6):419-431. doi:10.1038/nrd4309
- 600 5. Siramshetty VB, Nickel J, Omieczynski C, Gohlke BO, Drwal MN, Preissner R (2016)
601 WITHDRAWN--a resource for withdrawn and discontinued drugs. *Nucleic Acids Res* 44
602 (D1):D1080-1086. doi:10.1093/nar/gkv1192
- 603 6. Hopkins AL (2008) Network pharmacology: the next paradigm in drug discovery. *Nat Chem*
604 *Biol* 4 (11):682-690. doi:10.1038/nchembio.118
- 605 7. Anighoro A, Bajorath J, Rastelli G (2014) Polypharmacology: challenges and opportunities in
606 drug discovery. *J Med Chem* 57 (19):7874-7887. doi:10.1021/jm5006463
- 607 8. van Westen GJ, Wegner JK, Geluykens P, Kwanten L, Vereycken I, Peeters A, IJzerman AP, van
608 Vlijmen HW, Bender A (2011) Which compound to select in lead optimization? Prospectively
609 validated proteochemometric models guide preclinical development. *PLoS One* 6 (11):e27518.
610 doi:10.1371/journal.pone.0027518
- 611 9. Csermely P, Agoston V, Pongor S (2005) The efficiency of multi-target drugs: the network
612 approach might help drug design. *Trends Pharmacol Sci* 26 (4):178-182.
613 doi:10.1016/j.tips.2005.02.007
- 614 10. Fredholm BB (2010) Adenosine receptors as drug targets. *Exp Cell Res* 316 (8):1284-1288.
615 doi:10.1016/j.yexcr.2010.02.004
- 616 11. Fredholm BB, IJzerman AP, Jacobson KA, Linden J, Muller CE (2011) International Union of
617 Basic and Clinical Pharmacology. LXXXI. Nomenclature and classification of adenosine
618 receptors--an update. *Pharmacol Rev* 63 (1):1-34. doi:10.1124/pr.110.003285
- 619 12. Chen JF, Eltzschig HK, Fredholm BB (2013) Adenosine receptors as drug targets--what are the
620 challenges? *Nat Rev Drug Discov* 12 (4):265-286. doi:10.1038/nrd3955
- 621 13. Trudeau MC, Warmke JW, Ganetzky B, Robertson GA (1995) HERG, a human inward rectifier
622 in the voltage-gated potassium channel family. *Science* 269 (5220):92-95.
623 doi:10.1126/science.7604285
- 624 14. Milnes JT, Crociani O, Arcangeli A, Hancox JC, Witchel HJ (2003) Blockade of HERG
625 potassium currents by fluvoxamine: incomplete attenuation by S6 mutations at F656 or Y652.
626 *Br J Pharmacol* 139 (5):887-898. doi:10.1038/sj.bjp.0705335
- 627 15. Sanguinetti MC, Tristani-Firouzi M (2006) hERG potassium channels and cardiac arrhythmia.
628 *Nature* 440 (7083):463-469. doi:10.1038/nature04710
- 629 16. LeCun Y, Bengio Y, Hinton G (2015) Deep learning. *Nature* 521 (7553):436-444.
630 doi:10.1038/nature14539

- 631 17. Chen H, Engkvist O, Wang Y, Olivecrona M, Blaschke T (2018) The rise of deep learning in
632 drug discovery. *Drug discovery today*. doi:10.1016/j.drudis.2018.01.039
- 633 18. Gaulton A, Bellis LJ, Bento AP, Chambers J, Davies M, Hersey A, Light Y, McGlinchey S,
634 Michalovich D, Al-Lazikani B, Overington JP (2012) ChEMBL: a large-scale bioactivity
635 database for drug discovery. *Nucleic Acids Res* 40 (Database issue):D1100-1107.
636 doi:10.1093/nar/gkr777
- 637 19. Lenselink EB, Ten Dijke N, Bongers B, Papadatos G, van Vlijmen HWT, Kowalczyk W,
638 IJzerman AP, van Westen GJP (2017) Beyond the hype: deep neural networks outperform
639 established methods using a ChEMBL bioactivity benchmark set. *Journal of cheminformatics* 9
640 (1):45. doi:10.1186/s13321-017-0232-0
- 641 20. Liu X, Ye K, van Vlijmen HWT, IJzerman AP, van Westen GJP (2019) An exploration strategy
642 improves the diversity of de novo ligands using deep reinforcement learning: a case for the
643 adenosine A2A receptor. *Journal of cheminformatics* 11 (1):35. doi:10.1186/s13321-019-0355-
644 6
- 645 21. RDKit: Open-Source Cheminformatics Software. <http://www.rdkit.org>.
- 646 22. Rogers D, Hahn M (2010) Extended-connectivity fingerprints. *Journal of chemical information*
647 *and modeling* 50 (5):742-754. doi:10.1021/ci100050t
- 648 23. Scikit-Learn: machine learning in Python. <http://www.scikit-learn.org/>.
- 649 24. PyTorch. <https://pytorch.org/>.
- 650 25. Kingma DP, Ba J (2014) Adam: A Method for Stochastic Optimization. arXiv:1412.6980
- 651 26. Chung J, Gulcehre C, Cho K, Bengio Y (2014) Empirical Evaluation of Gated Recurrent Neural
652 Networks on Sequence Modeling. ArXiv:1412.3555
- 653 27. Deb K, Agrawal S, Pratap A, Meyarivan T A Fast Elitist Non-dominated Sorting Genetic
654 Algorithm for Multi-objective Optimization: NSGA-II. In: Schoenauer M, Deb K, Rudolph G
655 et al. (eds) *Parallel Problem Solving from Nature PPSN VI*, Berlin, Heidelberg, 2000// 2000.
656 Springer Berlin Heidelberg, pp 849-858
- 657 28. Emmerich MTM, Deutz AH (2018) A tutorial on multiobjective optimization: fundamentals
658 and evolutionary methods. *Nat Comput* 17 (3):585-609. doi:10.1007/s11047-018-9685-y
- 659 29. Liu X, IJzerman AP, van Westen GJP (2021) Computational Approaches for De Novo Drug
660 Design: Past, Present, and Future. *Methods Mol Biol* 2190:139-165. doi:10.1007/978-1-0716-
661 0826-5_6
- 662 30. Lameijer EW, Kok JN, Back T, IJzerman AP (2006) The molecule evaluator. An interactive
663 evolutionary algorithm for the design of drug-like molecules. *Journal of chemical information*
664 *and modeling* 46 (2):545-552. doi:10.1021/ci050369d
- 665 31. van der Horst E, Marques-Gallego P, Mulder-Krieger T, van Veldhoven J, Kruisselbrink J,
666 Aleman A, Emmerich MT, Brussee J, Bender A, IJzerman AP (2012) Multi-objective
667 evolutionary design of adenosine receptor ligands. *Journal of chemical information and*
668 *modeling* 52 (7):1713-1721. doi:10.1021/ci2005115
- 669 32. Nicolaou CA, Brown N (2013) Multi-objective optimization methods in drug design. *Drug*
670 *Discov Today Technol* 10 (3):e427-435. doi:10.1016/j.ddtec.2013.02.001
- 671 33. Solow AR, Polasky S (1994) Measuring biological diversity. *Environmental and Ecological*
672 *Statistics* 1 (2):95-103. doi:10.1007/BF02426650
- 673 34. Yevseyeva I, Lenselink EB, de Vries A, IJzerman AP, Deutz AH, Emmerich MTM (2019)
674 Application of portfolio optimization to drug discovery. *Information Sciences* 475:29-43.

675 doi:<https://doi.org/10.1016/j.ins.2018.09.049>
676 35. Sheridan RP (2013) Time-split cross-validation as a method for estimating the goodness of
677 prospective prediction. *Journal of chemical information and modeling* 53 (4):783-790.
678 doi:10.1021/ci400084k
679 36. Olivecrona M, Blaschke T, Engkvist O, Chen H (2017) Molecular de-novo design through deep
680 reinforcement learning. *Journal of cheminformatics* 9 (1):48. doi:10.1186/s13321-017-0235-x
681 37. Benjamin S-L, Carlos O, Gabriel L. G, Alan A-G (2017) Optimizing distributions over
682 molecular space. An Objective-Reinforced Generative Adversarial Network for Inverse-design
683 Chemistry (ORGANIC). doi:10.26434/chemrxiv.5309668.v3
684 38. Brown N, Fiscato M, Segler MHS, Vaucher AC (2019) GuacaMol: Benchmarking Models for
685 de Novo Molecular Design. *Journal of chemical information and modeling* 59 (3):1096-1108.
686 doi:10.1021/acs.jcim.8b00839
687
688

689 **Table S1: All tokens in vocabulary for SMILES sequence construction with RNN model.**

		Atoms					Bonds	Controls		
		Common Atoms			Aromatic Atoms		--	Rings	Branchs	On-Off
B	[Ag-3]	[CH-]	[N]	[SH2]	[b-]	[se+]	-	1	(GO
C	[As+]	[CH2]	[O+]	[SH]	[c+]	[se]	=	2)	EOS
F	[As]	[CH]	[O-]	[Se+]	[c-]	[te+]	#	3		
I	[B-]	[I+]	[OH+]	[SeH]	[cH-]	[te]		4		
L	[BH-]	[IH2]	[O]	[Se]	[n+]	b		5		
N	[BH2-]	[N+]	[P+]	[SiH2]	[n-]	c		6		
O	[BH3-]	[N-]	[PH]	[SiH]	[nH+]	n		7		
P	[B]	[NH+]	[S+]	[Si]	[nH]	o		8		
R	[C+]	[NH-]	[S-]	[Te]	[o+]	p		9		
S	[C-]	[NH2+]	[SH+]		[s+]	s				

690 Considering that the stereochemical information of molecules and ionic bonds were ignored, we removed
691 the “@”, “\”, “/”, “.”.

692 **Table S2: Comparison of validity, desirability, uniqueness and substructures distributions of**
 693 **SMILES generated by *DrugEx v2* with different ϵ in the multi-target and target-specific cases**
 694 **by using PF and WS rewarding schemes, respectively.** For the validity, desirability and
 695 uniqueness, the largest data is bold, while for the distribution of substructures, the bold data are
 696 labeled as the most closed to the values in the *LIGAND* set.

Case	Reward Scheme	Dataset / ϵ	Validity	Desirability	Uniqueness	Diversity	Purine Ring	Furan Ring	Benzene Ring
Multi-Target Case	PF	<i>LIGAND</i>	100.00%	14.63%	100.00%	0.67	21.30%	35.44%	79.24%
		10 ⁻²	99.39%	71.37%	90.47%	0.72	12.39%	34.69%	82.05%
		10 ⁻³	99.57%	80.81%	88.96%	0.71	13.97%	32.01%	80.26%
		10 ⁻⁴	99.72%	83.86%	87.19%	0.71	12.45%	30.58%	84.04%
		0	99.47%	73.76%	84.41%	0.70	13.35%	35.71%	81.89%
	WS	10 ⁻²	99.54%	87.56%	93.08%	0.60	9.66%	28.83%	92.19%
		10 ⁻³	99.80%	97.45%	93.44%	0.49	3.63%	21.06%	96.18%
		10 ⁻⁴	99.79%	98.15%	93.56%	0.53	2.89%	24.95%	91.46%
		0	99.78%	98.00%	90.19%	0.49	5.02%	16.45%	96.77%
		Target-Specific Case	PF	<i>LIGAND</i>	100.00%	12.40%	100.00%	0.66	28.27%
10 ⁻²	99.48%			88.76%	91.98%	0.77	18.31%	47.50%	68.95%
10 ⁻³	99.53%			89.49%	87.32%	0.72	23.73%	56.23%	67.40%
10 ⁻⁴	99.55%			91.84%	88.31%	0.74	26.86%	39.68%	74.36%
0	99.54%			91.47%	88.94%	0.75	22.95%	43.08%	71.50%
WS	10 ⁻²		99.16%	86.45%	93.97%	0.42	42.84%	97.26%	72.45%
	10 ⁻³		99.62%	97.86%	95.89%	0.31	60.81%	98.56%	51.87%
	10 ⁻⁴		99.67%	96.82%	94.56%	0.34	55.14%	93.69%	45.40%
	0		99.33%	96.28%	92.60%	0.35	42.86%	98.34%	63.47%

697

698

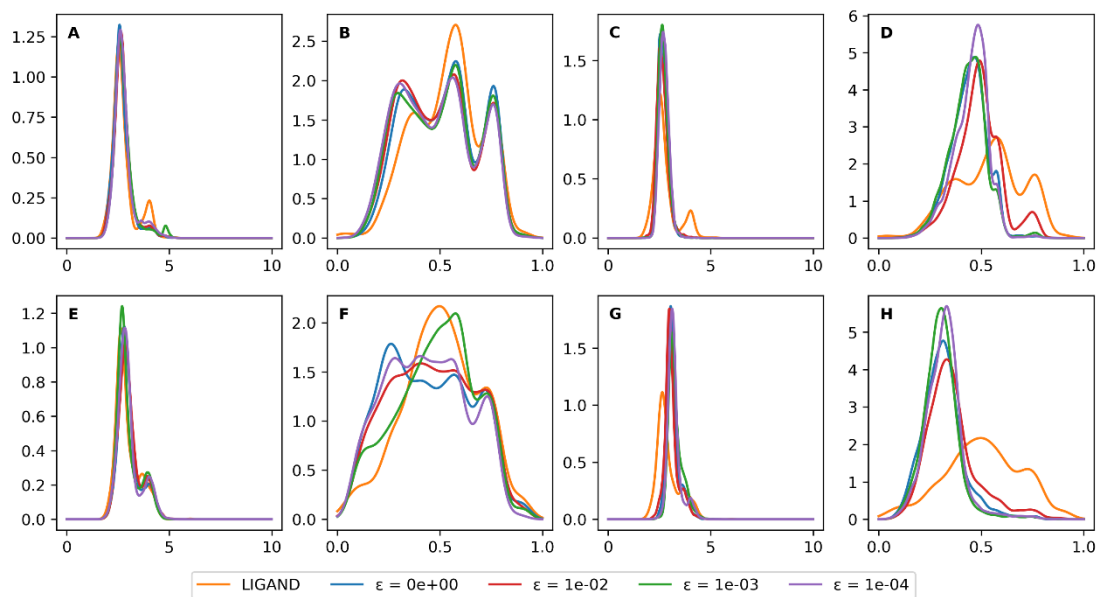
699 **Table S3: Results of the Goal-Directed tasks for our proposed method *DrugEx v2* and other baseline**700 **models on GuacaMol Benchmark.** GuacaMol platform contains 20 tasks with different requirements,701 including similarity, physicochemical properties, isomerism, scaffold matching, *etc.*. The results for

702 baseline models were cited from ref [38]. The bold data are shown as the best result for each task

703 achieved by different methods.

Benchmark	Best of Dataset	SMILES GA	Graph MCTS	Graph GA	SMILES LSTM	DrugEx v2
Celecoxib rediscovery	0.505	0.732	0.355	1	1	1
Troglitazone rediscovery	0.419	0.515	0.311	1	1	1
Thiothixene rediscovery	0.456	0.598	0.311	1	1	1
Aripiprazole similarity	0.595	0.834	0.38	1	1	1
Albuterol similarity	0.719	0.907	0.749	1	1	1
Mestranol similarity	0.629	0.79	0.402	1	1	1
C11H24	0.684	0.829	0.41	0.971	0.993	0.993
C9H10N2O2PF2Cl	0.747	0.889	0.631	0.982	0.879	1
Median molecules 1	0.334	0.334	0.225	0.406	0.438	0.418
Median molecules 2	0.351	0.38	0.17	0.432	0.422	0.435
Osimertinib MPO	0.839	0.886	0.784	0.953	0.907	0.967
Fexofenadine MPO	0.817	0.931	0.695	0.998	0.959	0.942
Ranolazine MPO	0.792	0.881	0.616	0.92	0.855	0.909
Perindopril MPO	0.575	0.661	0.385	0.792	0.808	0.812
Amlodipine MPO	0.696	0.722	0.533	0.894	0.894	0.898
Sitagliptin MPO	0.509	0.689	0.458	0.891	0.545	0.517
Zaleplon MPO	0.547	0.413	0.488	0.754	0.669	0.693
Valsartan SMARTS	0.259	0.552	0.04	0.99	0.978	0.978
Scaffold Hop	0.933	0.97	0.59	1	0.996	0.989
Deco Hop	0.738	0.885	0.478	1	0.998	0.986
Total	12.144	14.398	9.011	17.983	17.341	17.537

704



705

706 **Fig. S1:** the distribution of SA score and QED score of desired ligand in the *LIGAND* set and

707 molecules generated by *DrugEx v2* with different ϵ in the multi-target case (A-D) and target-

708 specific case (E-H) by using PR (A, B, E and F) and WS (C, D, G and H) rewarding schemes.

709